RSC Advances

Design of dual MMP-2/HDAC-8 Inhibitors by Pharmacophore Mapping, Molecular Docking, Synthesis and Biological Activity

Amit K. Halder[†], Sumana Mallick[‡], Deep Shikha[†], Achintya Saha[§], Krishna D. Saha[‡], and Tarun Jha*[†]

[†]*Natural Science Laboratory, Division of Medicinal and Pharmaceutical Chemistry, Department of Pharmaceutical Technology, P.O. Box 17020, Jadavpur University, Kolkata 700032, India*

[‡]*Cancer Biology & Inflammatory Disorder Division, CSIR-Indian Institute of Chemical Biology, Kolkata 700032, India*

[§]*Department of Chemical Technology, University of Calcutta, 92, APC Ray Road, Kolkata 700009, India*

[*]*Corresponding author: Tel: 9133 2457 2495 (o), 9133 2438 3814 (r), +919433187443 (m), e-mail: tjupharm@yahoo.com*

ABSTRACT

Recent analyses highlighted the promotion of cancer migration and invasion, mediated through HDAC via MMP-2 and MMP-9. Since both class 1 HDACs and MMP-2/9 are involved in the migration and invasion of cancer, an attempt has been taken to design dual MMP-2/HDAC-8 inhibitors by pharmacophore mapping and molecular docking approaches. The designed molecules were synthesized and showed a range of inhibitory activity against different MMP subtypes. Most of these designed compounds were selective towards MMP-2 but less potent against anti-targets like MMP-8, -12, etc. The highly active MMP-2 inhibitors were also found to be active towards HDAC-8 but less potent against other class 1 HDACs (HDAC-1 and -2). Molecular dynamics simulation revealed that the designed compounds may be acting through a distinct mechanism of action in the 'acetate ion channel' of HDAC-8. Some potent dual MMP-2/HDAC-8 inhibitors were further explored for *in vitro* cellular assay against human lung carcinoma cell line A549. These analyses revealed that some of these dual inhibitors have considerable anti-migratory and anti-invasive properties. The work may help to get some useful dual inhibitors.

Keywords: Matrix metalloproteinase, histone deacetylase, pharmacophore mapping, molecular dynamics, invasion assay.

1. INTRODUCTION

Matrix metalloproteinase is an important class of zinc-dependent endopeptidase involved in degradation of extracellular matrix (ECM) and remodelling of tissues[1-2]. So far, 28 different MMPs are known and are classified into six subgroups. Overexpression of MMPs are related to various pathological conditions such as cardiovascular, neurological, periodontal, central nervous system, emphysema, angiogenesis, metastatses as well as cancer[3-5]. Among all MMP subtypes, the MMP-2 (or gelatinase A) is considered as the most important target of cancer metastasis because of its strong correlation with cancer progression[6-8]. In last few decades, several attempts were made to design potential MMP-2 inhibitors as anticancer agents though none of these was successful in clinical trials. One of the major reasons for this failure is undesirable adverse effects caused by broad spectrum MMP inhibition[8-11]. On the other hand, histone deacetylases (HDACs) are another important class of metalloenzymes that catalyse deacetylation of N-terminal lysine residues of various proteins including nucleosomal histones[12-13]. The HDACs are involved in the chromatin assembly and remodelling, down-regulation of various gene expressions as well as DNA repair and re-combinations. Additionally, HDACs participate in various cellular processes by interacting with several non-histone proteins like transcription factors, molecular chaperones, cytoskeletal proteins, etc[13]. Due to these epigenetic and cellular functions, deregulation of HDACs leads to several pathological conditions including cancer[12, 14-15]. Eighteen different isotypes of HDACs are identified and classified into four subgroups - class I (HDAC1-3 and 8), class II (HDAC4-7, 9 and 10), class III (sirtuins 1-7) and class IV (HDAC11). Among these, over-expression of class 1 HDACs is associated with various human cancers. Several attempts were made in last few years to develop class I HDAC inhibitors. Two of these inhibitors, suberoylanilide hydroxamic acid (SAHA or varinostat) and the FK228 (romidepsin) have already been approved by US food and Drug administration (US FDA) for the treatment of cutaneous T cell lymphoma whereas some other inhibitors are under clinical trial[16-18]. Most of these HDAC inhibitors are pan-inhibitors (non-selective towards specific isoform). Selectivity towards specific HDAC isoform is preferable but not essential criteria for HDAC inhibitor design[14, 19].

Both HDACs and MMPs are related to cancer migration, invasion and metastases[20-22]. Moreover, HDAC inhibitors suppress MMP-2 activation and lung cancer cell invasion via RECK protein upregulation[23]. Similar suppression of migration and invasion was found in breast carcinoma cell lines where HDAC inhibition led to the downregulation of both MMP-2 and MMP-9[24]. Furthermore, HDAC-1, -6 and -8 have been found to suppress MMP-9 to inhibit

breast cancer cell invasion[22]. Therefore, dual MMP-2/HDAC-8 inhibitors may be potential candidates to impart the higher anti-migratory and anti-invasive properties of cancer cells than the selective MMP or the selective HDAC inhibitor. Such designing of dual inhibitor is complicated since both these metalloenzymes have several isoforms, and broad spectrum inhibition (especially MMPs) may give rise to undesirable adverse effects. Ideally, these inhibitors should specifically block the targets responsible for invasion and metastases (such as MMP-2, MMP-9) and spare anti-targets (like MMP-8, -12, etc). Design of dual MMP-2/HDAC-8 inhibitors has earlier been explored by Cheng et al though the cellular effect or isoform selectivity of these inhibitors was not described[25]. In the current study, we attempted to design novel dual MMP-2/HDAC-8 inhibitors by pharmacophore mapping techniques, with an aim to investigate the potency of these inhibitors on lung cancer cell migration and invasion. Due to structurally distinct active site of HDAC-8, most broad spectrum HDAC inhibitors are least potent against this enzyme[14]. Therefore, the HDAC-8 remains as the least investigated class 1 HDAC isoform as far as its biological functions are concerned. The HDAC-8 knockdown was earlier reported to suppress cell proliferation in lung, cervical, colon and neuroblastoma cell lines. Moreover, invasion of HDAC-8 transfected cells was found to be higher than HDAC-1 transfected cells[22]. Presently, more than 20 human ligand-bound HDAC-8 protein structures are available that may serve as good starting points for the generation of the structure-based pharmacophore models[26]. In the current investigation, the designed dual MMP-2/HDAC-8 inhibitors were synthesized, screened against different MMP and HDAC isoforms to understand their potency and selectivity as well as tested against human lung cancer cell line A549 for cytotoxicity. Finally, migration and invasion assays were performed for the active compounds against A549 human lung carcinoma cell line which highly expresses both MMP-2 and HDAC-8. Immunofluorescence assay was also done for cellular MMP-2 expression followed by molecular dynamics (MD) studies.

2. RESULTS AND DISCUSSION

2.1. Development of pharmacophore model

Pharmacophore mapping is one of the most essential tools for development of anticancer agents[27-29]. For the design of the dual MMP-2/HDAC-8 inhibitors, pharmacophore models were developed and validated for both these enzymes separately. The development and validation of pharmacophore models for MMP-2 inhibitors were reported earlier[11], where the best ligand-based pharmacophore (Hypo 2) was generated with one hydrophobic (H), one hydrogen bond

acceptor (A) and two hydrogen bond acceptor lipid (AL) features (Figure S2, supporting information).

In the current study, ligand- and structure-based pharmacophore models for HDAC-8 inhibitors were developed. The details of model development and validation are discussed in the supporting information (Text S1). Briefly, a dataset[30-34] containing 111 reported HDAC-8 inhibitors (Table S1, supporting information) was selected and structurally diverse 24 molecules (Figure S1) of this dataset were used to build the ligand-based pharmacophore models. The remaining 87 compounds were used as the test set to validate the developed models. For development of the structure-based pharmacophore, X-ray crystal structure of HDAC-8 (PDB: 1VKG)[35-36] was used. The best ligand-based pharmacohore (LigPharm01, Text S1, supporting information) was generated with acceptor (A), hydrophobic aromatic (H_{Ar}) and zinc binding (Z) features (Figure 1a), whereas the best structure-based pharmacophore (StrPharm02, Text S1, supporting information) comprises of two ring aromatic (Ra), one hydrophobic (H) and one zinc binding features (Figure 1b). These pharmacophore models of MMP-2 and HDAC-8 were used for the design of their dual inhibitors.

<center>**[Figure 1 may be placed here]**</center>

2.2. Design of dual MMP-2 and HDAC-8 inhibitors

Previously, the molecular modeling studies of MMP-2 inhibitors were reported[11]. In that MMP-2 inhibitor dataset[11], some compounds were designed from antineoplaston (A-10) metabolite N2-phenylacetyl L-isoglutamine (AS2-5), and those derivatives showed variable MMP-2 inhibitory activities[37-38]. The AS2-5 derived MMP-2 inhibitors contained either the benzoyl[37] or the phenylacryloyl[38] moieties conjugated with L(+)-isoglutamine. The best active molecules of these two series[37-38] were considered for designing a hypothetical molecule (to retain the structural information of MMP-2 inhibition) that would map all features of the StrPharm02 (so that HDAC-8 inhibitory activity of this hypothetical molecule may be ensured). The design and structure of the hypothetical molecule (**H1**, 4(S)-5-(benzylamino)-4-(2-(4-methoxyphenyl)acetamido)-5-oxopentanoic acid) is shown in Figure 2. The **H1** was found to map all features of StrPharm02 [Figure 1b]. Furthermore, this compound showed the predicted HDAC-8 inhibitory activity (IC_{50}) of 3.5 μM when mapped with LigPharm01 [Figures 1a]. Both these mappings indicated that the **H1** may be a potential inhibitor of HDAC-8 enzyme. Furthermore, the mapping of the **H1** in the best ligand-based pharmacophore of MMP-2 (Hypo2)[11] provides a predicted activity (IC_{50}) of 40.5 μM (pIC_{50} = 4.392) [Figure 2]. Therefore, the pharmacophore mapping analyses indicated that **H1** may be considered as a virtual hit for

<center>4</center>

dual MMP-2/HDAC-8 inhibition. To confirm this hypothesis, **H1** was synthesized and its activity was determined against both MMP-2 and HDAC-8. The IC_{50} activities against MMP-2 and HDAC-8 were found to be 83.7 µM (pIC_{50} = 4.077) and 3.8 µM, respectively. Since the MMP-2 inhibitory activity of the molecule was not found to be satisfactory, **H1** was subjected to tailoring and a series of derivatives and analogs (compounds **D1-D35**), structurally similar to **H1** were synthesized for lead modification purpose. The activity of these derivatives and analogs was first screened against MMP-2 enzyme. The best active compounds were identified and were further evaluated with other MMPs (MMP-1,-8,-9,-12,-14). The most suitable derivatives were tested against HDAC-8 enzyme as well as the nuclear extract of HELA cells containing HDACs (rich in HDAC-1 and -2).

[Figure 2 may be placed here]

The design of the modified leads (**D1-D35**) was done on the basis of the molecular docking prediction. The **H1** was docked in the protein structure of MMP-2 (PDB: 1HOV)[39] using quantum polarized ligand docking (QPLD) tool[40-41]. The best docked pose (Dockscore: -8.907) is illustrated in Figure 3. It is found that the methoxyphenyl moiety of **H1** interacts with His85 and Asp72 by pi-pi and pi-anion interactions respectively whereas the benzyl moiety is inserted into the hydrophobic S1' cavity to form pi-pi interaction with His120 and pi-charge interactions with the catalytic zinc atom. Interestingly, no interaction is observed with the methoxy group of **H1**. These interactions are consistent with the docking interactions observed by Li et al[38]. Since the methoxyphenyl residue of **H1** is exposed to the hydrophilic atmosphere, the higher activity of these compounds depends largely on the charge transfer (pi-pi and pi-anion) interactions. Therefore, the substitution of this phenyl moiety should be more favourable for the charge transfer reactions with residual amino acids. Since both pi-pi and pi-anion interactions may be possible, the charge transfer interactions are difficult to predict in this case. Therefore, the R_1 groups of the designed molecule were selected in a way so that the variable electron densities of the adjacent phenyl residue may be achieved to alter these charge transfer interactions. Since the other unsubstituted benzyl residue of **H1** is involved in the charge transfer interactions at the S1' cavity, increase in the hydrophobic as well as charge transfer interactions should alter the biological activity. To understand the important interactions for the higher biological activity, the R_2 group of the designed molecule was substituted with different aliphatic and aromatic residues. It is worth mentioning that the binding interactions of the S1' pocket have been thoroughly investigated earlier. Devel et al[9, 10] reported that the bulky aromatic substitutions in this cavity increase MMP-2 inhibitory activity in several folds at the loss of

isoform selectivity towards MMP-2. Moreover, such substitutions may increase the activity of these molecules towards MMP-8 and MMP-12 which are considered as anti-targets for cancer treatment. Therefore, such bulky substitutions were avoided during the design of **H1** and its modified leads (**D1-D35**). In addition, Lipinski[42] and Veber[43] rules were also taken into consideration during this design. Although Veber rules were relaxed in some cases, Lipinski rule (except molecular weight<500) was strictly followed.

[Figure 3 may be placed here]

2.3.   Syntheses and enzymatic assay of the designed compounds

The designed compounds (**D1-D35**) were synthesized through the route outlined in Scheme 1.

[Scheme 1 may be placed here]

The synthesized compounds (**D1-D35**) are listed in Table 1. The MMP-2 inhibitory activity of these derivatives was tested and the IC_{50} value is also depicted in Table 1.

[Table 1 may be placed here]

It is evident from Table 1 that the 4-chloro- and the 4-bromophenyl and the naphthalene derivatives are the most suitable among other substitutions. The long straight aliphatic chains at the R_2 position are mostly favourable than both the short and the branched aliphatic chains. Although the benzyl substitution at the R_2 position shows the higher activities but the phenyl substitution at the same position is unfavourable. The benzyl and n-hexyl moieties at the R_2 position are more active than other analogs. Initially, compounds **D1-D29** were synthesized to understand these SARs. After confirming **D11** as the most active MMP-2 inhibitor of this series (**D1-D29**), the R_2 position was substituted with different benzyl residues to obtain **D30-D35** in order to further improve the MMP-2 inhibitory activity. This decision was monitored by the docking interaction of **D11**, provided in the Supporting information (Figure S3). The docking pose (Dockscore: -9.681) suggested that the hydrophobic and the charge transfer interactions at the S1' pocket have high impact on the biological activity of these compounds. Compounds **D30-D35** showed variable MMP-2 inhibitory activity. Substitution of the R_2 position with the 4-nitrobenzyl (**D33**) and the 2-chlorobenzyl (**D35**) derivatives showed the higher MMP-2 inhibition than **D11**. The other analogs exhibited the similar or the lower activity comparing to that of **D11**. The **D33** was found to be the highest active MMP-2 inhibitor (IC_{50} = 6.40 μM) in the current series.

Fourteen compounds of the current series (**D1, D4, D11, D12, D24-D25, D28-D35**) were selected for further investigations. These compounds were evaluated for their inhibitory

activities towards MMP-1, -8, -9, -12 and -14 to understand the selectivity profiles. The inhibitory potentials of these compounds towards HDAC-8 and the nuclear HDACs were also determined. These enzyme inhibitory activities are presented in Table 2.

[Table 2 may be placed here]

It is observed that the most of these compounds are non-selective towards other MMPs like MMP-1, MMP-8, MMP-12 and MMP-14. The MMP-8 is considered as an antitarget for cancer treatment and the inhibition of it may give rise to undesirable adverse effects[7, 8]. The MMP-12 has also been reported to be an antitarget since its inhibition may increase angiogenesis and lung metastases. The exact disease context of MMP-14 is unknown but inhibition of it may lower tumour growth, angiogenesis and metastases[8]. Though the MMP-9 or gelatinase-B is closely associated with cancer progression, inhibition of this enzyme may develop adverse effects in advanced stage of disease[6, 21]. Noticeably, the activity of the designed compounds towards MMP-9 varied to a considerable extent. Although these compounds showed a range of activities for different MMPs, the HDAC-8 inhibitory activity of these derivatives was almost similar. The IC_{50} of HDAC-8 of all compounds except **D29** (52.56 µM) is lower than 10 µM. Interestingly, all these compounds were found to be selective towards HDAC-8 as compared to HELA nuclear extract of HDACs (rich in HDAC1 and 2). On the basis of these enzymatic expressions, four compounds (**D11**, **D29**, **D33** and **D35**) were finally selected for cellular assays. These compounds were tested for their anti-proliferative, anti-migratory and anti-invasive properties against A549 cells.

2.4. Cytotoxicity and flow cytometry apoptotic assays

Compounds **D11**, **D29**, **D33** and **D35** were tested for cytototoxicity against A549 cells by 3-(4,5-dimethylthiazol-2-yl)-2,5-diphenyltetrazolium bromide (MTT) assay. The cytotoxicity assay [Figure 4(A)] depicted that none of these dual inhibitors are highly cytotoxic in nature. These showed negligible cytotoxicity (5-25%) at the lower concentrations (50-100 µM). Only at the higher concentrations (300 µM), these showed perceptible changes in cell viabilities (35-44%). To check the involvement of apoptosis for anti-proliferative effects, annexin V-PI flow cytometry analyses were conducted with two derivatives, **D11** and **D29**. Two lower dose concentrations (50 and 100 µM) were selected for these cytometry analyses. The results are presented in Figure 4(B-F). It demonstrates that these compounds show minimal apoptotic as well as necrotic effects on the cells. The purpose of these cytotoxicity and flow cytometry analyses was to select an appropriate non-cytotoxic dose for the migration and invasion assays. Both these assays are performed in non-cytotoxic doses where the migration and invasion

properties may not be affected by the cytotoxicity of these compounds[21]. From these analyses, 50 µM dose was selected for both the migration and invasion assays.

[Figure 4 may be placed here]

2.5. Migration assay

The anti-migratory properties of the selected derivatives (compounds **D11**, **D29**, **D33** and **D35**) were tested by the wound healing assay. The A549 cells were treated with 50 µM of these compounds (except the control) for 48 hours after a scratch was made on the monolayer of cells. The observations are illustrated in Figure 5(A). It demonstrates extensive migration of the untreated cells (control) in previously created denuded area. The migration of the compound treated cells varied considerably; the most prominent anti-migratory effect was noted for **D33**. The antimigratory effect of **D11** was lower than **D33** but higher than other two derivatives, **D29** and **D35**.

[Figure 5 may be placed here]

2.6. Invasion assay

Inhibition of A549 cell invasion by these derivatives (**D11**, **D29**, **D33** and **D35**) was estimated through fluorimetric QCM ECMatrix cell invasion assay (ECM 555, Millipore). The percentages of invaded cells are graphically presented in Figure 5(B). The inhibition was the most prominent for **D33** which showed 38-42% reduction in cell invasion. The **D11** reduced the invasion upto 33-34%. The other two compounds failed to show such inhibition. Compounds **D35** and **D29** showed inhibition of 16-18% and 10-13%, respectively. Thus, from both the migration and the invasion assays, it may be confirmed that **D33** and **D11** are two most promising candidates in the current series. Interestingly, both these compounds showed comparatively higher activity against MMP-9 enzyme. These results indicate that the higher MMP-9 inhibition along with MMP-2 and HDAC-8 are proportional to the higher anti-migration and anti-invasion properties of these compounds. These results may validate the findings of previously reported investigations[22, 24] that highlighted HDAC mediated upregulation of both MMP-2 and MMP-9 in the increase of cancer cell invasion.

2.7. Immunofluorescence assay for cellular MMP-2 expression

To understand the potency of the designed compounds for lowering the cellular MMP-2 expression, immunofluorescence microscopy technique was used to analyze the cellular expressions of MMP-2 enzyme after the compound treatment. For nucleus counterstaining, 4'-6-diamidino-2-phenylindole (DAPI) was used. The expressions of MMP-2 antibodies in untreated control and treated cells are represented in Figure 6 along with phase contrast, DAPI

and merged MMP-2/DAPI images. The intensity of the MMP-2 antibody expressions was measured by ImageJ tool[44]. It is observed that the expression of the cellular MMP-2 is reduced by both **D33** and **D11**; compound **D33** reduced the expression of MMP-2 up to 40%, whereas **D11** showed 30% reduction after 24 hours comparing with that of the control.

[Figure 6 may be placed here]

2.8. Molecular dynamics (MD) simulation analysis

In vitro analyses confirmed that **D33** was active against both HDAC-8 and MMP-2. To get insights into its mechanisms of action, **D33** was docked at the binding sites of MMP-2 (PDB: 1HOV)[39] and HDAC-8 (PDB:1VKG)[35] enzymes separately. The best docked poses were selected (Dockscore, MMP-2: -10.026 and HDAC-8:-7.899), and the docked complexes (MMP-2:**D33** and HDAC-8:**D33)** were subjected to MD simulations at 10 ns separately. The root mean square deviation (RMSD) and root mean square fluctuation (RMSF) diagrams of both complexes are provided in the supporting information (Figure S4). These observations demonstrate stabilities of these complexes during 10 ns simulation. The ligand-protein contacts of these two complexes are illustrated in Figure 7. In both MD simulation runs, the carboxyl group of **D33** was found to interact strongly with the catalytic zinc atom of both of HDAC-8 and MMP-2 enzymes. For MMP-2 complex, His120 made a strong pi-pi interaction with the nitrophenyl residue of **D33**. Noticeably, all amino groups of **D33** were involved in the polar interactions with the catalytic amino acid residues. This compound made hydrogen bond interactions with Leu83 and Gly81 with the occurrences of 65% and 71%, respectively. Water bridged interaction with Pro140 residue was also observed with a low percentage (27%). The lower number of interactions in the S1' pocket may explain the higher selectivity towards MMP-2 enzyme as well as the variations in the MMP inhibitory activities of the designed compounds. On the other hand, **D33** produced multiple hydrogen bond interactions with Cys153, His143 and Tyr306 residues of HDAC-8 protein. The 4-bromophenyl residue of **D33** made pi-pi interactions with Trp141 and Arg37. Interestingly, Tpr141 is non-conserved amino acid in HDAC-8 and the tryptophan residue is replaced by leucine residue in HDAC1-3[45-46]. The selective inhibition of HDAC-8 is possible through interactions with the amino acid residues present in the internal 'acetate release channel' of this enzyme[47]. This 'acetate release channel' is smaller in HDAC-8 than other HDACs. This work also showed that the released acetate ion (after reaction of HDAC-8 with lysine) is stabilized by Trp141 and Arg37 and this mechanism is unique in HDAC-8. Therefore, interactions with one of these amino acids may lead to the selective inhibition of HDAC-8 enzyme. Such interactions are found in the X-ray

crystal structures of the HDAC-8 (PDB IDs:3SFF and 3SFH)[47] [supporting information (Figure S5)], where HDAC-8 selective inhibitors interact strongly with Trp141 by pi-pi interactions. The **D33**, on the other hand, was found to interact with both Trp141 and Arg37, and these interactions may be responsible for its isoform specificity towards HDAC-8. The histogram and timeline interaction diagrams of HDAC-8:**D33** complex are provided in supporting information (Figure S6). These diagrams reveal that **D33** made several interactions with the amino acid residues (Ile34, His143, Phe152, Cys153 and Tyr306) present in the 'acetate release channel' of HDAC-8. These interactions may also contribute to the higher isoform specificity of **D33**.

[Figure 7 may be placed here]

3. CONCLUSION

In the current report, the design, syntheses and biological activities of dual MMP-2/HDAC-8 inhibitors have been presented. Pharmacophore-based technique is adopted for the design of these dual inhibitors. The pharmacophore models correctly predicted the activity of the designed molecules. The models may be used for development of the higher active molecules for these targets. Apart from the observed activity against MMP-2 and HDAC-8, the selectivity of the designed molecules against other MMPs and HDACs were taken into consideration. It was observed that the best active molecules were selective towards specific MMP (i.e., MMP-2) and HDAC (HDAC-8) but less active against other MMPs (i.e., MMP-8, MMP-12, MMP-1, etc) that are considered as anti-targets of cancer treatment[7, 8]. Since the scopes of MMP-2[3-5] and HDAC-8 inhibitors[16] are not limited to cancer, the designed molecules may be further studied to understand the aspects of these molecules for other diseases. Moreover, the active HDAC-8 inhibitors may be studied for anti-proliferative activity against T-lymphocyte cells[48]. Since, both MMP-2 and HDACs are involved in the cancer cell migration and invasion, the inhibitory potentials of the dual inhibitors towards A549 lung carcinoma cell migration and invasion were explored. The designed compounds provide a range of MMP-2 inhibitory activities whereas the HDAC-8 inhibition is almost constant for the higher active dual inhibitors. Molecular dynamics simulation revealed that the designed compounds may be acting through a distinct mechanism of action through the 'acetate ion channel' of HDAC-8. These provide a scope to understand the role of different MMPs and HDACs for migration and invasion of cancer cell. It was also observed that compounds simultaneously inhibiting MMP-2, MMP-9 and HDAC-8 were more active than compounds having activity against one or two of these enzymes. This finding partially validates the mechanism of HDAC-8 mediated progress of cancer cell invasion via

MMP-9. These analyses may be taken into consideration to design the potential dual inhibitors in future.

4. MATERIALS AND METHODS

4.1. Computational Chemistry

4.1.1. Ligand-based pharmacophore mapping

All ligand structures were prepared by *Prepare ligand for QSAR* tool of Discovery Studio (DS)[49] where duplicate structures of these compounds were removed and the pH of these molecules was set to 7.4. These structures were subsequently minimized by Smart Minimizer algorithm (Max steps: 10000, RMS gradient: 0.01) and *Distance dependent dielectric* implicit solvent method using CHARMm input forcefield. Hypogen algorithm[50] was used to develop 3D-QSAR pharmacophore models using DS[49] considering zinc binding feature (Z) as a mandatory feature for the hypothesis generation. The detail procedure is similar described in previous work[51].

4.1.2. Structure-based pharmacophore mapping

The pharmacophore hypotheses generation was carried out on different PDB structures of human HDAC-8 complexes following the protocols outlined in previous work (except maximum charge distance that was set at 5.6)[51]. Two validation procedures were implemented - (1) selectivity score based ranking approach and (2) the decoy set validation. The active and confusing decoy set compounds were collected from DUD-E database (http://dude.docking.org)[51-52] and the rest of the validation procedures were similar to previously reported methods[51].

4.1.3. Quantum polarized ligand docking (QPLD)

Since both MMPs and HDACs are the metalloenzymes having catalytic zinc metal, accurate docking estimation requires quantum mechanics (QM) level treatment. Therefore, quantum polarized ligand docking (QPLD) technique[53] was used to dock the designed inhibitors into the active site of these metalloenzymes. The NMR structure of MMP-2 enzyme (PDB ID: 1HOV)[39] and X-ray crystal structure of HDAC-8 (PDB ID:1VKG)[35] were obtained from the PDB[36]. The receptor structures were described using OPLS force field parameters. The partial charges and the protonation states of the receptor molecules were described using Epik module and the catalytic zinc atom was assigned with +2 atomic charge. The restrained minimization of hydrogen atoms of these protein molecules was performed by the *protein preparation wizard* using OPLS2005 force field. A receptor grid box (size 15Å x15Åx 15Å) was generated considering the bound ligands of the respective protein as a centre of the box[54]. The initial

docking of the prepared ligands was performed using the standard precision (SP) protocol to generate the preliminary ligand poses. The single point calculation of the ligand poses using the density functional theory (DFT) based Becke-Lee-Yang-Parr (BLYP)/6-31G* model was done to calculate the polarizable charges of these inhibitors. These charges were assigned for the inhibitors by electrostatic potential (ESP) fitting. Finally, these inhibitors with new partial charges were re-docked into the enzyme active site to obtain the most energetically favourable ligand poses. The best pose of the ligands was selected from the highest Dockscore value.

4.1.4. Molecular dynamic (MD) simulation

The MD simulation of the protein-ligand complexes was carried out through Desmond/Maestro[54]. The detailed protocols of MD simulation were described previously[51]. The protein complexes were simulated for 10 ns with a step of 2 fs NPT ensemble. The Nose-Hoover chain thermostat and Martyna-Tobias-Klein barostat were used to maintain temperature and pressure at 300 K and 1.013 bar respectively. The atomic coordinate data and system energies were measured every 10 ps recording the trajectory at 4.8 ps[51, 55].

4.2. Organic chemistry

4.2.1. General

The mass spectroscopy (MS) analysis was performed through a LC MS/MS [(The LC, Agilent 1290-column, Model G1316C (Agilent Technologies), Wellplate Sampler 1290-ALS, Model G4226A; Binary pump 1290-Bin Pump, Model G4220A] coupled to electrospray ion (ESI) mass spectrometer (MS QQQ) of multimode system, controlled through Mass Hunter Quantitative Analysis software. The ^{1}H nuclear magnetic resonance (NMR) spectra were measured on a AC bruker 300 mHz FT-NMR machine with TMS as the internal standards after dissolving these compounds in dimethyl sulphoxide-d6 (DMSO-d6) solvent (Chembridge Isotope Laboratories Inc., USA). Infrared spetroscopy (IR) analyses were performed in a Bruker alpha 11960095 FT-IR instrument. Splitting patterns are designated as s (singlet), d (doublet) and m (multiplet). The HMBC analysis was performed with a Bruker Avance DPX-500 spectrometer using DMSO-d6 solvent. Optical rotation of these compounds was observed by Perkin-Elmer Type 141 polarimeter. Melting point of all synthesized compounds was measured on Mel-Temp electrothermal apparatus and a capillary melting point apparatus and was further verified in CTRONICS-a digital melting point apparatus. Reactions were monitored by the analytical thin layer chromatography (TLC) performed on silica gel G plates (TLC silica gel 60 F$_{254}$, Merck, Germany). Spots were visualized by keeping the TLC plates in ultraviolet

(UV) light (254 nm) or placing the plates in iodine vapour. The column chromatography was performed using 200-300 mesh silica gel with appropriate solvent systems. All solvents were reagent grade and when necessary were purified or dried by standard methods.

4.2.2. Syntheses
The designed compounds were synthesized by following the methods earlier proposed by Li et al[37-38] with appropriate modifications. The general synthetic technique was outlined in Scheme 1.

Syntheses of substituted phenylacetyl chlorides/napthylacetyl chloride (I1-I9)
Substituted phenyl acetic acid/naphthyl acetic acid (0.1 mol) (**S1**-**S9**) and benzene (50-60 ml) were taken separately in 250 ml round bottomed flask. The flask was fitted with a reflux condenser attached with a calcium chloride drying tube and a dropping funnel. Thionyl chloride (0.4-0.5 mole) was added drop-wise from the dropping funnel to the round bottomed flask under anhydrous condition. The reaction mixture was refluxed for 3-4 hr until HCl gas evaluation stops. The evolution of HCl gas was checked by congo red paper. The excess of thionyl chloride was removed by distillation with three 50 ml portions of dry benzene to obtain the products (**I1-I9**) which were used immediately in the next reaction without further purifications.

Syntheses of 2-N-(substituted phenylacetyl)-L(+)-isoglutamic acids (I10-I17) and 2-N-napthylacetyl-L(+)-isoglutamic acid (I18)
L(+)-Glutamic acid (0.1 mol) was taken in a 250 ml conical flask. Sodium hydroxide solution (2N) was added slowly to the conical flask till all glutamic acid dissolved and the mixture become slightly alkaline (pH 7.5-8.0). The reaction mixture was stirred on a magnetic stirrer with the temperature maintained at 0-5°C. Maintaining the alkalinity, the substituted phenylacetyl chlorides/napthylacetyl chlorides (**I1-I9**) were added individually in small portions to the reaction mixture with constant stirring, and sodium hydroxide (2N) was added time-to-time to keep the reaction mixture alkaline. The reaction end points were monitored by TLC. After the completion of the reaction, the reaction mixture was washed with 10-15 ml of benzene or diethyl ether. The aqueous solutions were then acidified with 6N HCl in ice cold condition to precipitate the solid products at the bottom and the solution was kept cooled for about ½-1hr to allow more precipitations. The precipitated products were filtered, washed several time with distilled water and dried as much as possible under vacuum. These were again washed with 15-20 ml of benzene and dried to obtain the solid products (**I10-I18**). All

these intermediate products were purified by recrystallization with warm water. Physical data of intermediate compounds (**I10-I18**) are shown in Table S2 in the supporting information.

2(S)-5-(benzylamino)-4-(2-(4-chlorohenyl)acetamido)-5-oxopentanoic acid (D1)

A mixture of 2(S)-2-(2-(4-chlorophenyl)acetamido)pentanedioic acid (**I10**) and 50-60 ml of dry chloroform was taken in a 250 ml flat bottom flask. The reaction mixture was stirred on a magnetic stirrer with the temperature maintained at 0-5°C under anhydrous condition. The N,N-dicyclohexylcarbidiimide (DCC) (0.01 mol) was dissolved in 20 ml dry chloroform and it was added slowly and gradually to the reaction mixture with continuous stirring. After 1h of stirring, benzyalmine (0.02 mol) was added to the reaction mixture and it was continuously stirred for 5-6 h. After the reaction was over, the reaction mixture was kept in the refrigerator for overnight. The solution was filtered and both the solid part [dicyclohexylurea (DCU)] and the liquid (chloroform) layer were extracted with cold 1N sodium carbonate (Na_2CO_3) solution. The aqueous part was then acidified to pH 2 with 1N HCl in cold condition to obtain solid precipitations of these products separately. These solid products were extracted with ethyl acetate (3x30 ml) and were dried with anhydrous Na_2SO_4 overnight. The solvents were subsequently removed under reduced pressure and the resulting crude residues were recrystallized from ethanol and dried to obtain the target compounds (**D1**) as white solid. Yield: 47.8%. MP 143-145^{0}C. MS (ESI Postive) m/z [M+Na$^+$] 407.21.^{1}H NMR (DMSO-d6, 300 mHz, ppm) δ12.09 (s, 1H, COOH), δ 8.40 (m, 1H, CONH), δ 8.17 (d, 1H, CONH, J=8.31), δ6.80 (d, 9H, Benzene); δ 4.26 (m, 1H, CH), δ 4.24 (m, 2H, CH$_2$), δ 3.70 (s, 3H, OCH$_3$); δ 3.38 (s, 2H, CH$_2$), δ 2.15 (m, 2H, CH$_2$), δ 1.86 and 1.74 (m, 2H, CH$_2$).IR (KBr, cm-^{1}):3319 (N-Hstr of CONH), 3065 (aromatic =C-H str), 2960 (assym. aliphatic -C-H str), 2858 (sym. aliphatic -C–H str), 1723 (C=O str COOH), 1647 (C=O str of CONH), 1619 (aromatic C=C str), 1541 (N-H deformation), 1435 (aliphatic -C-H deformation), 1414, 1266 (C-O str and O-H bending of COOH). The NMR spectra of **I10** and **D1** are provided in the supporting information (Figure S7 and S8). The HMBC spectra of **D1** are also provided in the supporting information (Figures S9). For **D1**, cross peaks were found between N5-H (8.43) and C4 (171.22), N3-H (4.24) and C4 (171.22) as well as C7-H (2.15) and C8 (173.87). However, no cross-peak was found between N5-H (8.43) and C8 (173.87). The current results are consistent with the observation of Li et al[38].

The other final products were synthesized according to the general procedure as described for the syntheses of **D1.** The details of spectral analyses are provided in supporting information (Text S2).

14

4.3. Biology

4.3.1. Matrix metalloproteinase inhibition assay
The MMPs inhibition assays were carried out using MMP inhibitor profiling kits, purchased from Enzo Life Science International, Inc., Plymount Meeting, PA, USA, following the manufacturer's protocol. The concentration of chromogenic substrates was detected by its absorbance value at 410 nm in a microplate photometer (Thermo Scientific Multiscan FC, USA). Enzyme reactions were performed at $37^{o}C$ for 1 h in a 100 µl final volume of solutions with at least six concentrations of inhibitors (except the control) in triplicate. After addition of the substrate, the increase of absorbance was recorded in 1 min time intervals for 30 minutes (except for MMP-12, 60 mins) at 410 nm with the help of a microplate photometer (Thermo Scientific Multiscan FC, USA). An inhibitor, N-isobutyl-N-(4-methoxyphenylsulfonyl)glycyl hydroxamic acid (NNGH) was included as a prototype control inhibitor. The concentration of compounds that provide 50% inhibition of enzymatic activity (IC_{50}) was determined by semi-logarithmic dose–response plots (Graph Pad Prism 5.0 for Windows, Graph Pad Software Inc., San Diego, California, USA, 2007).

4.3.2. HDAC-8 inhibition assay
The HDAC-8 inhibitory activities of these designed compounds were determined by using the *Fluor-de-Lys* HDAC-8 activity assay kit (Enzo Life Sciences International, Inc., Plymount Meeting, PA, USA) according to the manufacturer's protocol. . The fluorescence was measured with a multi-mode microplate reader at 380 nm excitation and 460 nm emission (SpectraMax, Molecular Devices, USA) spectra. Inhibition of HDAC-8 activity was monitored by a decrease in fluorescence signal.

4.3.3. HDAC-1/2 inhibition assay
The activity of the designed compounds towards other class 1 HDACs was estimated using *Color-de-lys* HDAC activity assay kit (Enzo Life Sciences International, Inc., Plymount Meeting, PA, U.S.A.) that contain the nuclear extract of HELA cells. This nuclear extract is rich in HDAC1 and HDAC2. The HDAC-8 is found in this extract in a very low to negligible amount. The assay was performed according to manufacturer's protocol. The absorbance was measured at 410 nm by a microplate photometer (Thermo Scientific Multiscan FC, USA).

4.3.4. Cytotoxicity assay
The lung carcinoma cell line A549 was maintained as monolayer cultures in Dulbecco's Modified Eagle Medium (DMEM) (Gibco) supplemented with 10% heat-inactivated FBS (Invitrogen, USA) and Penicillin-Streptomycin (100 IU ml^{-1} -100 µg ml^{-1}). The anti-

proliferative activity of the compound was evaluated by MTT assay. Briefly, cells were seeded into 96-well plates at 5000 cells per well, and allowed to adhere for 18-24 h prior to addition of these compounds separately. The designed synthesized compounds (diluted with serum free DMEM media) were added in different concentrations and kept for 48 h. 10 µl of MTT solution (10 mg ml^{-1}) was added to each well before 4 h at the end of incubation,. After 4 h of incubation, the formazan crystals were solubilised in 100 µl of DMSO. The absorbance was measured at 570 nm using a microplate photometer (Thermo Scientific Multiscan FC, USA). The viability was calculated by considering the control containing the solvent control (0.1% DMSO) to be 100% viable.

4.3.5. Flow cytometry apoptosis assay

The apoptosis assay was done by using an annexin V-FITC apoptosis detection kit (Calbiochem, Germany). Briefly, cells were treated with different concentrations of compounds and were stained with propidium iodide (PI) and annexin V-FITC according to the manufacturer's instructions. The percentage of the live, apoptotic and necrotic cells were analyzed by BD LSR Fortessa cell analyzer (Becton Dickinson, USA). Data from 10^6 cells were analyzed for each sample.

4.3.6. Would healing migration assay

The A549 cells were plated in 24 well plate at a density of 5×10^4 cells per well with the complete media (DMEM + 10% FBS). After 60-70% confluence, these cells were starved overnight. A straight scratch was made in the cell monolayer by 20-200 µl pipette tip. The detached as well as loosely adhered cells were washed thrice with PBS. These cells were then treated with different concentrations of the designed compounds for 48 h and then photographed.

4.3.7. Invasion assay

The anti-invasiveness of the synthesized compounds was evaluated by a fluorimetric QCM ECMatrix Cell Invasion Assay kit (Millipore, USA). The assay was performed in a 96-well invasion plate based on Boyden chamber principle. The A549 cells were starved overnight in FBS-free DMEM, followed by harvesting and placing 1×10^5 cells (resuspended in FBS-free medium with 5% BSA) in each well.of the insert. The lower portion of the chamber is called the feeder tray that contained the medium with 5% FBS as a chemo-attractant. The synthesized compounds were added to the cell suspensions in triplicates. These cells were incubated in the absence (untreated) as well as in the presence of these compounds at fixed concentrations (50 µM) for 24 hrs. Invasive cells are able to invade through a basement layer of matrix membrane

solution and cross the pores of polycarbonate membranes to adhere at the bottom of the inserts. The adhered cells were dissociated with cell detachment solution and the detached cells were detected by CyQuantGR dye. The fluorescence was measured with a multi-mode microplate reader at 480 nm excitation and 520 nm emission (SpectraMax, Molecular Devices, USA) spectra.

4.3.8. Immunofluorescence assay

Anti-MMP-2 antibody (sc-10736) and CFL-tagged secondary antibody (sc-362252, IgG-CFL 488) were purchased from Santa Cruz Biotechnology, Inc, USA. The A549 cells were seeded into glass cover slips at a density of 1×10^6 cells/cm^2 and treated with these compounds (except the control). After 24 h, these cells were fixed with 4% paraformaldehyde in PBS for 15 min, permeabilized with 0.1% Triton X-100 in PBS for 20 min and exposed to the blocking solution (PBS containing 5% bovine serum albumin and 0.2% Tween 20) for 1 h at room temperature. The fixed cells were then incubated overnight with anti-MMP-2 primary antibody (1:250 dilutions), washed with PBS and subsequently treated with secondary antibody (1:250 dilutions) for 1 h. For nuclear localization, the culture was then treated with 10 mg/ml of DAPI solution for 1 min. Samples were mounted in Vectashield hard set mounting media (Vector Laboratories, USA). Cells were observed under an Andor spinning disk confocal microscope and images were acquired. The corrected total cell fluorescence (CTCF) was measured by ImageJ tool[44]. All integrated density of each cells (presented in these images) and at least six background areas were measured and CTCF value was determined as per eq. (1).

CTCF = [Integrated desnity - (area of selected cell x mean fluorescence of background readings)]   (1)

ACKNOWLEDGEMENTS

ABBREVIATIONS USED

DS: Discovery studio software; FT-IR: Fourier transform infrared spectroscopy; HDAC: Histone deacetylase; HMBC: Heteronuclear multiple bond correlation; MMP: Matrix metalloproteanse; MP: Melting point; MS: Mass spectrometry; NMR: Nuclear magnetic resonance; QPLD: Quantum polarized ligand docking; QSAR: Quantitative structure activity relationship; RMSD: Root mean square deviation; RMSF: Root mean square fluctuation

REFERENCES

1. C. Tallant, A. Marrero and F. X. Gomis-Ruth. *Biochim. Biophys. Acta,* 2010, **1803**, 20-28.

2. K. Kessenbrock, V. Plaks and Z. Werb. *Cell,* 2011, **141**, 52–67.

3. A. M. Venkatesan, J. M. Davis, G. T. Grosu, J. Baker, A. Zask, J. I. Levin, J. Ellingboe, J. S. Skotnicki, J. F. Dijoseph, A. Sung, G. Jin, W. Xu, D. J. McCarthy and D. Barone. *J. Med. Chem.,* 2004, **47**, 6255-6269.

4. R. P. Verma and C. Hansch. *Bioorg. Med. Chem.,* 2007, **15**, 2223-68.

5. V. Vargova, M. Pytliak and V. Mechirova, in *Matrix metalloproteanases*; ed S. P. Gupta, Springer, Basel, 1st edn., 2012; ch. 4, pp. 1-33.

6. E. I. Deryugina and J. P. Quigley. *Biochim. Biophys. Acta,* 2010, **1803**, 103-120.

7. C. M. Overall and O. Kleifeld. *Nature Rev.,* 2006, **6,** 227-239.

8. A. Defour and C. M. Overall. *Trends Pharm. Sci.* 2013, **34**, 233-242.

9. L. Devel, S. Garcia, B. Czarny, F. Beau, E. Lajeunesses, L. Vera, D. Georgiadia, E. Stura and V. Dive. *J. Biol. Chem.,* 2010, **285**, 35900-35909.

10. L. Devel, F. Beau, M. Amoura, L. Vera, E. Cassar-Lajeunesse, S. Garcia, B. Czarny, E. A. Stura and V. Dive. *J. Biol. Chem.,* 2012, **287**, 26647-26656.

11. A. K. Halder, A. Saha and T. Jha. *J. Pharm. Pharmacol.,* 2013, **65**, 1541-1554.

12. B. Barneda-Zahonero and M. Parra. *Mol. Oncol*., 2012, **6**, 579-89.

13. M. A. Glozak, N. Sengupta, X. Zhang and E. Seto, *Gene,* 2005, **363,** 15-23.

14. L. Zhang, Y. Han, Q. Jiang, C. Wang, X. Chen, X. Li, F. Xu, Y. Jiang, Q. Wang and W. Xu. *Med. Res. Rev.,* 2015, **35**, 63-84.

15. A. A. Lane and B. A. Chabner. *J .Clin. Oncol.,* 2009, **27**, 5459-5468.

16. S. Valente and A. Mai. *Expert Opin. Ther. Pat.,* 2014, **24***,* 401-15.

17. J. M. Wagner, B. Hackanson, M. Lubbert and M. Jung. *Clin. Epigenetics.* 2010, **1,** 117-136.

18. M. Guha. *Nat. Rev. Drug Discov.,* 2015, **14**, 225-226.

19. S. Balasubramanian, E. Verner and J. J. Buggy. *Cancer Lett.,* 2009, **280**, 211-221.

20. K. Mittal, J. Ebos and B. Rini. *Semin. Oncol.,* 2014, **41**, 235-251.

21. B. Fabre, K. Filipiak, J. M. Zapico, N. Diaz, R. J. Carbajo, A. K. Schott, M. P. Martinez-Alcazar, D. Suarez, A. Pineda-Lucena, A. Ramos and B. de Pascual-Teresa. *Org. Biomol. Chem.,* 2013, **11**, 6623-6641.

22. S. Y. Park, J. A. Jun, K. J. Jeong, H. J. Heo, J. S. Sohn, H. Y. Lee, C. G. Park and J. Kang. *Oncol. Rep.,* 2011, **25**, 1677-1681.

23. L. T. Liu, H. C. Chang, L. C. Chiang and W. C. Hung. *Cancer Res.,* 2003, **63**, 3069-3072.

24. H. W. Jeon and Y. M. Lee. *Mol. Cancer Ther.,* 2010, **9***,* 1361-70.2010

25. X. C. Cheng, R. L. Wang, Z. K. Dong, J. Li, Y. Y. Li and R. R. Li. *Bioorg. Med. Chem.,* 2012, **20**, 5738-5744.

26. X. Hou, J. Du, R. Liu, Y. Zhou, M. Li, W. Xu and H. Fang. *J. Chem. Inf. Model.,* 2015, **55**, 861-871.

27. A. K. Halder, A. Saha and T. Jha. *Curr. Top. Med. Chem.,* 2013, **13**, 1098-1126.

28. S. Y. Yang. *Drug Discov. Today,* 2010, **15**, 444-50.

29. A. R. Leach, V. J. Gillet, R. A. Lewis and R. Taylor. *J. Med. Chem.,* 2010, **53**, 539-558.

30. Y. Zhang, J. Feng, C. Liu, L. Zhang, J. Jiao, H. Fang, L. Su, X. Zhang, J. Zhang, M. Li, B. Wang and W. Xu. *Bioorg. Med. Chem.,* 2010, **18**, 1761-1776.

31. Y. Zhang, J. Feng, C. Liu, H. Fang and W. Xu. *Bioorg. Med. Chem.,* 2011, **19**, 4437-4444.

32. Y. Zhang, J. Feng, Y. Jia, Y. Xu, C. Liu, H. Fang and W. Xu. *Eur. J. Med. Chem.,* 2011, **46**, 5387-5397.

33. Y. Zhang, C. Liu, C. J. Chou, X. Wang, Y. Jia and W. Xu. *Chem. Biol. Drug Des.,* 2013, **82**, 125-130.

34. Y. Zhang, H. Fang, J. Feng, Y. Jia, X. Wang and W. Xu. *J. Med. Chem.,* 2011, **54***,* 5532-5539.

35. J. R. Somoza, R. J. Skene, B. A. Katz, C. Mol, J. D. Ho, A. J. Jennings, C. Luong, A. Arvai, J. J. Buggy, E. Chi, J. Tang, B. C. Sang, E. Verner, R. Wynands, E. M. Leahy, D. R. Dougan, G. Snell, M. Navre, M. W. Knuth, R. V. Swanson, D. E. McRee and L. W. Tari. *Structure*, 2004, **12**, 1325-1334.

36. H. M. Berman, J. Westbrook, Z. Feng, G. Gilliland, T. N. Bhat, H. Weissig, I. N. Shindyalov and P. E. Bourne. *Nucleic Acids Res.,* 2000, **28**, 235-242.

37. X. Li, J. Wang, J. Li, J. Wu, Y. Li, H. Zhu, R. Fan and W. Xu. *Bioorg. Med. Chem.,* 2009, **17**, 3053-3060.

38. X. Li, Y. Wang, J. Wu, Y. Li, Q. Wang and W. Xu. *Bioorg. Med. Chem.,* 2009, **17**, 3061-3071.

39. Y. Feng, J. J. Likos, L. Zhu, H. Woodward, G. Munie, J. J. McDonald, A. M. Stevens, C. P. Howard, G. A. De Crescenzo, D. Welsch, H. S. Shieh and W. C. Stallings. *Biochim. Biophys. Acta.,* 2002, **1598**, 10-23.

40. A. E. Cho and D. Rinaldo. *J. Comp. Chem.,* 2009, **30**, 2609-2616.

41. V. Librando and M. Pappalardo, *J. Mol. Graph. Model.,* 2013, **44**, 1-8.

42. C. A. Lipinski, F. Lombardo, B. W. Dominy and P. J. Feeney. *Adv. Drug Delivery Rev.,* 1997, **23**, 2-25.

43. D. F. Veber, S. R.Johnson, H-Y. Cheng, B. R. Smith, K. W. Ward and K. D. Kopple. *J. Med. Chem.,* 2002, **45**, 2615-2623.

44. C. A. Schneider, W. S. Rasband and K.W. Eliceiri. *Nat. Methods*, 2012, **9**, 671-675.

45. S. Di Micco, M. G. Chini, S. Terracciano, I. Bruno, R. Riccio and G. Bifulco. *Bioorg. Med. Chem.,* 2013, **21**, 3795-3807.

46. A. Vannini, C. Volpari, G. Filocamo, E. C. Casavola, M. Brunetti, D. Renzoni, P. Chakravarty, C. Paolini, R. De Francesco, P. Gallinari, C. Steinkuhler and S. Di Marco. *Proc. Natl. Acad. Sci.,* 2004, **101**, 15064-15069.

47. L. Whitehead, M. R. Dobler, B. Radetich, Y. Zhu, P. W. Atadja, T. Claiborne, J. E. Grob, A. McRiner, M. R. Pancost, A. Patnaik, W. Shao, M. Shultz, R. Tichkule, R. A. Tommasi, B. Vash, P. Wang and T. Stams, *Bioorg. Med. Chem.,* 2011, **19**, 4626-4634.

48. S. Balasubramanium, J. Ramos, W. Luo, M. Sirisawad, E. Verner and J. J. Buggy. *Leukemia*, 2008, **22**, 1026-1034.

49. Accelrys Inc., Discovery Studio 3.0, San Diego, USA, 2011.

50. H. Li, J. Sutter and R. Hoffmann, in Pharmacophore Perception, Development, and Use in Drug Design. ed O. F. Güner, International University Line, CA, 2000, ch 10, pp. 173-189.

51. A. K. Halder, A. Saha, K. D. Saha and T. Jha. *J. Biomol. Str. Dyn.,* 2015*, 33*, 1756-1779.

52. N. Huang, B. K. Scoichet and J. J. Irwin. *J. Med. Chem.,* 2006, **49***, 6789-6801.

53. Schrödinger Suite 2011 QM-polarized ligand docking protocol; Glide version 5.7; Jaguar version 7.8, QSite version 5.7, Schrödinger, LLC, New York, NY, 2011.

54. K. J. Bowers, E. Chow, H. Xu, R. O. Dror, M. P. Eastwood, B. A. Gregersen, J. L. Klepis, I. Kolossvary, M. A. Moraes, F. D. Sacerdoti, J. K. Salmon, Y. Shan and D. E. Shaw. *Proceedings of the ACM/IEEE Conference on Supercomputing (SC06)*, Tampa, Florida, November 11–17, 2006.

55. C. Mondal, A. K. Halder, N. Adhikari and T. Jha. *Mol. Divers.,* 2014, **18**, 655-671.

Figure captions

Figure 1. Interfeature distance constraints of (a) LigPharm01 and (b) StrPharm02.

Figure 2. Design of dual MMP-2/HDAC-8 inhibitors from pharmacophore mapping analyses. A: hydrogen bond acceptor, H: hydrophobic, Ra: ring aromatic, AL: hydrogen bond acceptor lipid, Z: zinc binding feature.

Figure 3. Best docking pose of compound **H1**; left side: three-dimensional (3D) representation with hydrophobic contour map, hydrophobic contour map is shown as higher to lower as brown to blue (▬▬ ▬▬); right side: 2D representation of the docking interactions, colours are as follows (● charged (negative), ● charged (positive), ● hydrophobic, ● metal, ● polar, ➤ hydrogen bond (backbone), •• pi-pi interaction, — salt bridge, ● solvent exposure)

Scheme 1. Reagents and conditions: (a) $SOCl_2$ in benzene; (b) L(+)-glutamic acid, 2N NaOH (pH 7.5-8.5), then 1N HCl; (c) DCC, $CHCl_3$; (d) RNH_2, 1N Na_2CO_3, 1N HCl

Figure 4. (A) Antiproliferative activity of higher active MMP-2/HDAC-8 inhibitors. The results of annexin-V/PI binding assay through flow cytometry for (B) untreated control, (C) D11 (50 μM), (D) D11 (100 μM), (E) D29 (50 μM), (F) D29 (100 μM)

Figure 5. Results of (A) wound healing migrtion assay and (B) Matrigel invasion assay of active designed molecules.

Figure 6. Confocal miscroscopy images of cellular MMP-2 expressions in untreated, compounds **D11** and **D33** treated A549 cell lines.

Figure 7. The percentage occurrence of interactions observed in 10 ns MD simulations of **D33** complex of (A) MMP-2 and (B) HDAC-8.
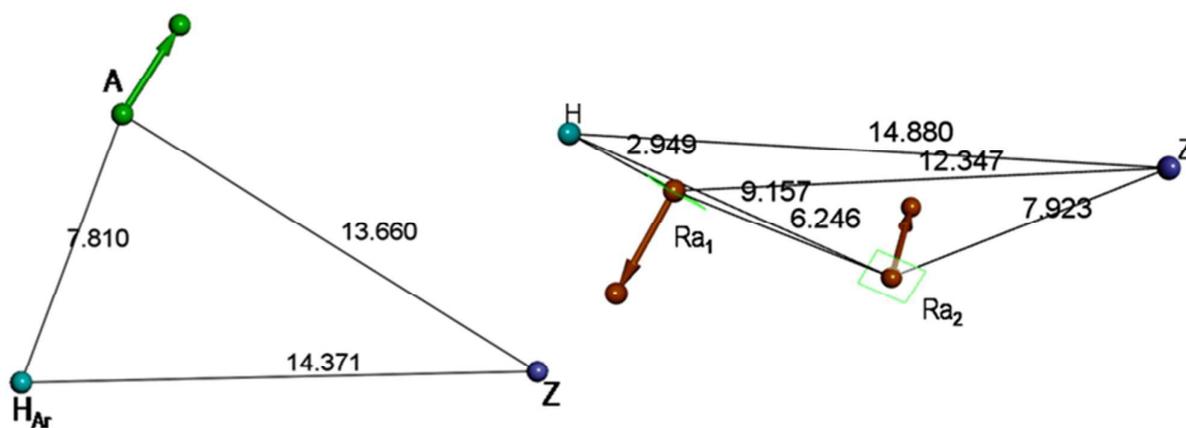
Figure 1
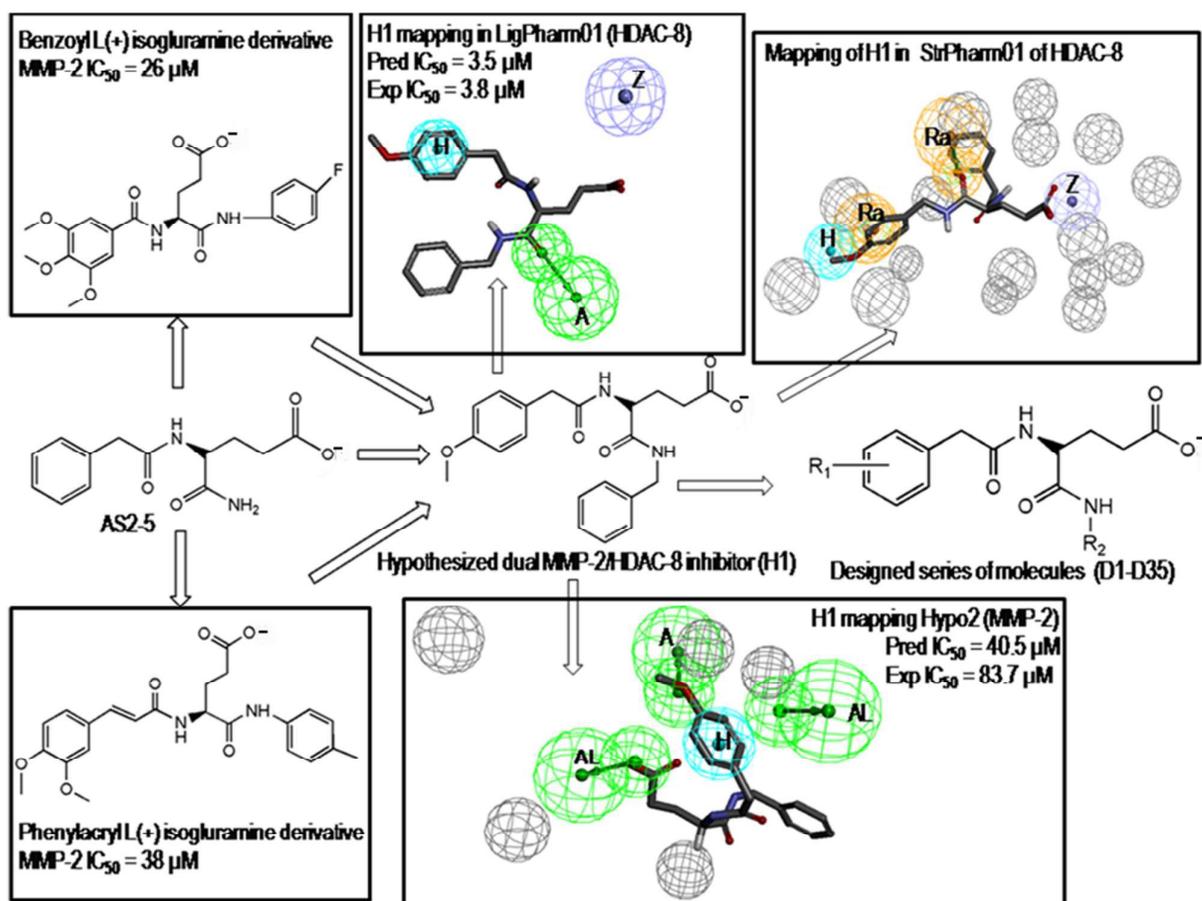
Figure 2
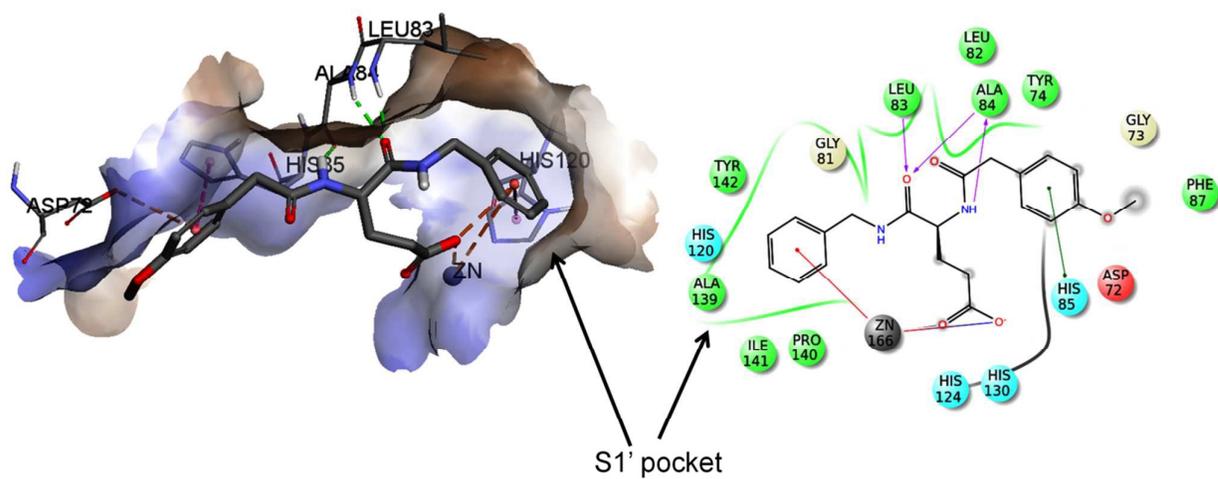
Figure 3

Scheme 1

Figure 4

(A)

(B)
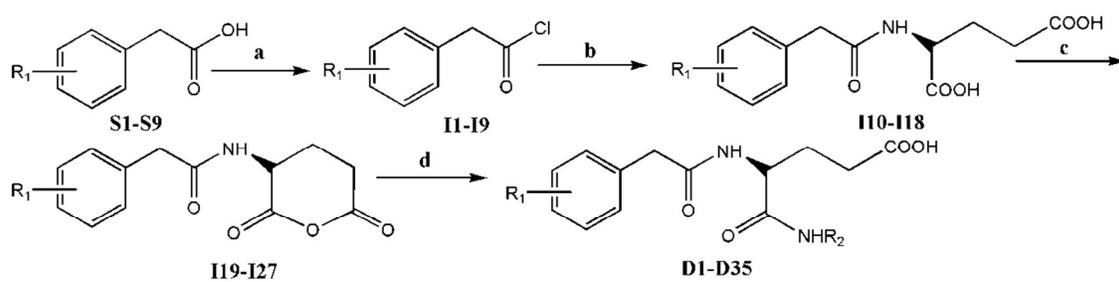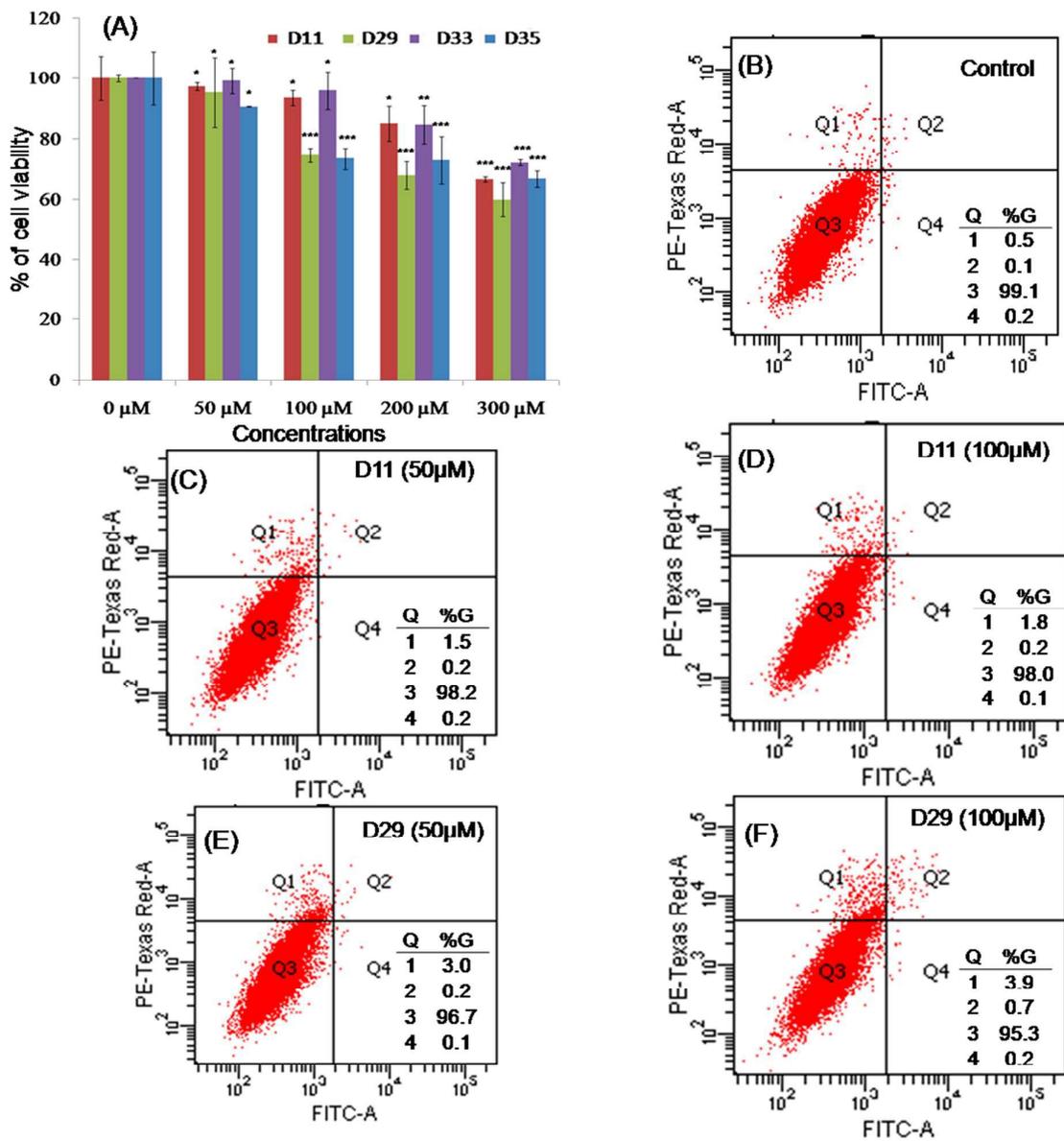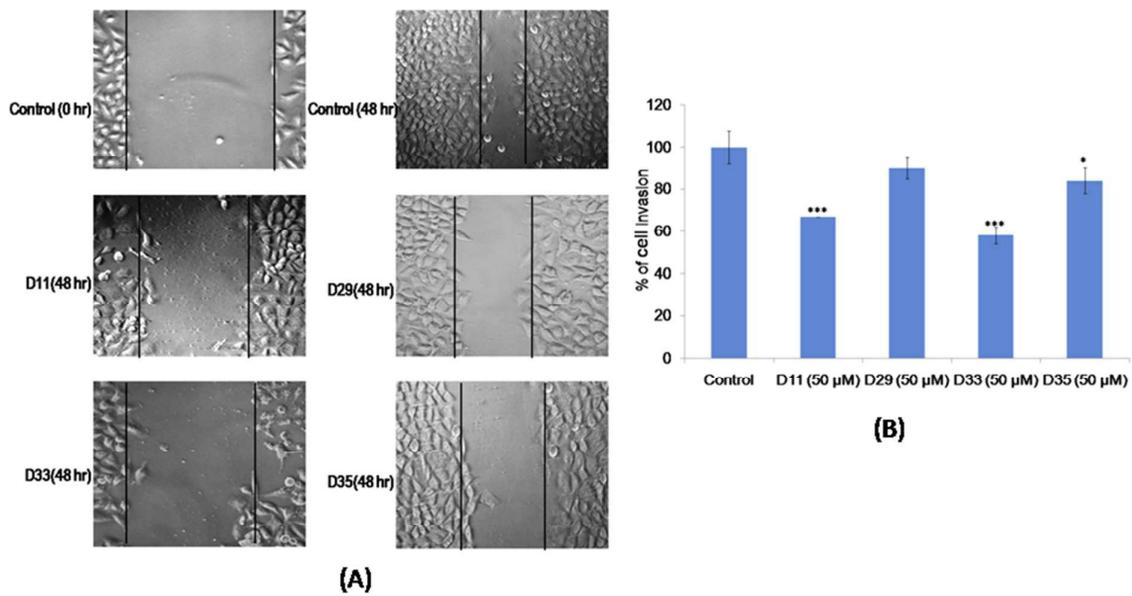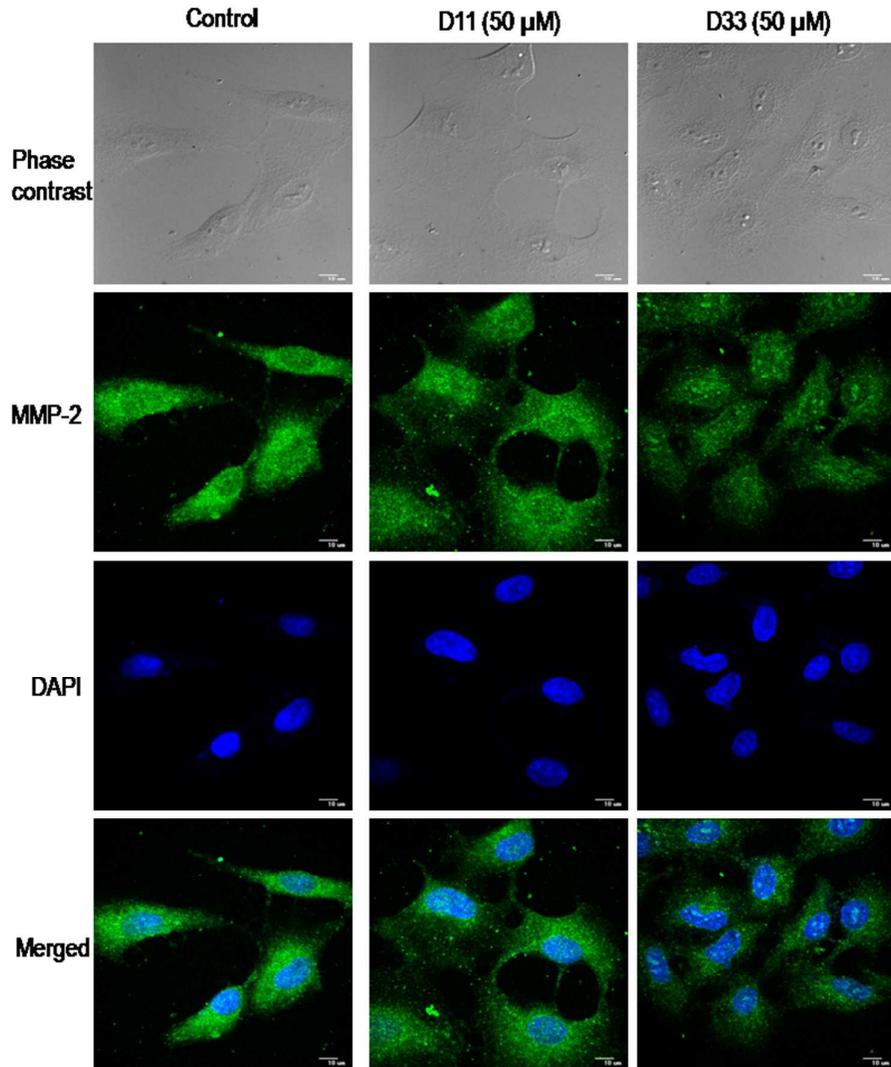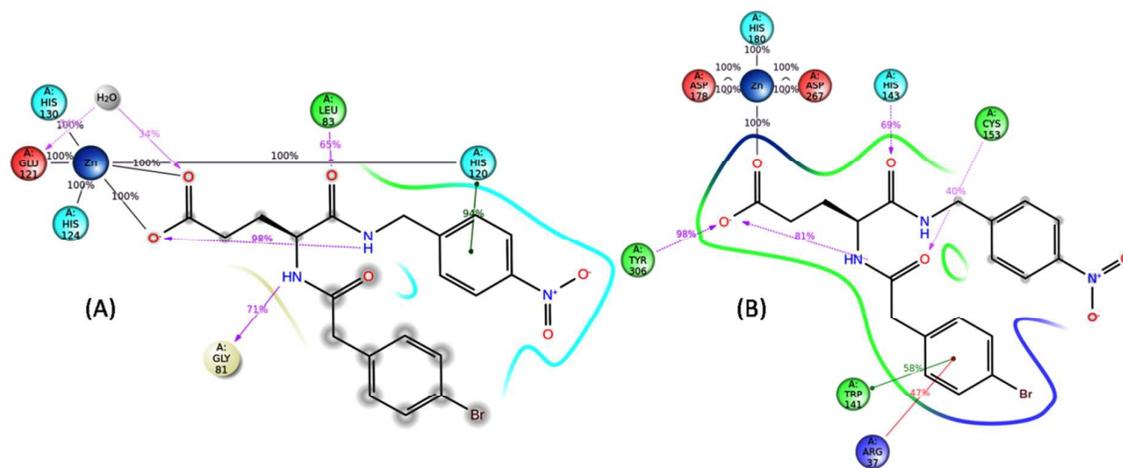
Figure 5

Figure 6

Figure 7

Table 1. Structures and MMP-2 inhibitory activity of the designed molecules.
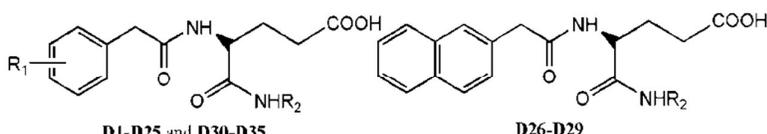
Cpd.	R_1	R_2	MMP-2 (IC_{50}) (μM)
D1	4Cl	$CH_2C_6H_5$	37.60
D2	4Cl	i-C_4H_9	199.53
D3	4Cl	n-C_4H_9	141.25
D4	4Cl	n-C_6H_{13}	44.60
D5/H1	$4OCH_3$	$CH_2C_6H_5$	83.75
D6	$4OCH_3$	i-C_4H_9	81.03
D7	$4NO_2$	n-C_5H_{11}	57.90
D8	$4NO_2$	t-C_4H_9	101.60
D9	4Br	i-C_3H_7	105.40
D10	4Br	n-C_5H_{11}	73.15
D11	4Br	$CH_2C_6H_5$	19.60
D12	4Br	n-C_6H_{13}	39.40
D13	2Cl	i-C_4H_9	78.60
D14	2Cl	$CH_2C_6H_5$	66.60
D15	2Cl	i-C_3H_7	76.40
D16	2Cl	n-C_5H_{11}	86.90
D17	2Br	i-C_3H_7	177.83
D18	2Br	i-C_4H_9	84.30
D19	2Br	n-C_5H_{11}	110.60
D20	2Br	C_6H_5	162.18
D21	2F	n-C_4H_9	140.60
D22	2F	n-C_5H_{11}	80.40
D23	2F	C_6H_5	151.36
D24	2,4-diCl	$CH_2C_6H_5$	71.50
D25	2,4-diCl	n-C_6H_{13}	23.10
D26	-	t-C_4H_9	88.00
D27	-	i-C_3H_7	91.42
D28	-	$CH_2C_6H_5$	43.40
D29	-	n-C_6H_{13}	6.50
D30	4Br	$CH_2C_6H_4$ 4-Cl	23.30
D31	4Br	$CH_2C_6H_4$ 4-F	42.40
D32	4Br	$CH_2C_6H_3$ 3,4Cl_2	49.70
D33	4Br	$CH_2C_6H_4$ 4-NO_2	6.40
D34	4Br	$CH_2C_6H_4$ 4-OCH_3	38.30
D35	4Br	$CH_2C_6H_4$ 2-Cl	7.70

Table 2. MMPs and HDACs inhibitory activities of the designed compounds

Cpd.	MMP-1	MMP-2[a]	MMP-8	MMP-9	MMP-12	MMP-14	Nuclear HDACs	HDAC-8
				IC$_{50}$ (µM)				
D1	>250	37.6	207.67	5.2	238	45.83	>100	3.33
D4	>250	44.6	169.53	57.82	>250	73.92	>100	5.02
D11	**>250**	**19.6**	**201.05**	**8.9**	**94.52**	**23.56**	>100	**3.03**
D12	>250	39.4	240.32	74.57	199.73	100.32	>100	4.21
D24	>250	71.5	101.53	63.06	>250	85.6	>100	6.07
D25	>250	23.1	168.23	83.1	>250	85.79	>100	8.6
D28	>250	43.4	230.4	74.57	>250	90.19	>100	6.05
D29	**>250**	**6.5**	**183.89**	**81.36**	**>250**	**98.69**	>100	**52.56**
D30	>250	23.3	205.75	64.82	168.98	91.99	>100	4.09
D31	>250	42.4	244.53	70.42	132.31	83.16	>100	4.27
D32	>250	49.7	208.02	>250	>250	193.35	>100	4.45
D33	**>250**	**6.4**	**205.89**	**4.83**	**138.32**	**56.33**	>100	**2.89**
D34	>250	38.3	180.83	5.64	50.56	99.29	>100	5.09
D35	**>250**	**7.7**	**181.63**	**86.01**	**68.78**	**102.67**	>100	**6.29**

[a]For comparison